# Cardiovirus leader proteins retarget RSK kinases toward alternative substrates to perturb nucleocytoplasmic traffic

Belén Lizcano-Perret[1], Cécile Lardinois[1], Fanny Wavreil[1], Philippe Hauchamps[2], Gaëtan Herinckx[3], Frédéric Sorgeloos[1], Didier Vertommen[3], Laurent Gatto[2] and Thomas Michiels[1*]

[1] VIRO unit, de Duve Institute, Université Catholique de Louvain, Brussels, Belgium

[2] CBIO unit, de Duve Institute, Université Catholique de Louvain, Brussels, Belgium

[3] PHOS unit and MASSPROT platform, de Duve Institute, Université Catholique de Louvain, Brussels, Belgium

[*]Corresponding author: thomas.michiels@uclouvain.be (TM)

# Abstract

Proteins from some unrelated pathogens, including viruses and bacteria can recruit and activate cellular p90-ribosomal protein S6 kinases (RSKs) through a common linear motif. Our data suggested that such pathogens' proteins might act as adapters to dock the kinase toward specific substrates. We explored this hypothesis using the *Cardiovirus* leader protein (L) as a paradigm. L is known to trigger phenylalanine-glycine nucleoporins (FG-NUPs) hyperphosphorylation and nucleocytoplasmic trafficking perturbation. Using a biotin ligase fused to either RSK or to L, we identified FG-NUPs as primary partners of the L-RSK complex in infected cells. Mutant analysis shows that L uses distinct motifs to recruit RSK and to dock the L-RSK complex toward the FG-NUPs. Using an analog-sensitive RSK2 mutant kinase, we show that, in infected cells, L can trigger RSK to use NUP98 and NUP214 as direct substrates. Our data illustrate a novel virulence mechanism where pathogens' proteins retarget cellular protein kinases toward specific substrates.


# Introduction

Proteins encoded by several unrelated pathogens, including RNA viruses, DNA viruses and bacteria, were recently shown to use a common short linear motif (D/E-D/E-V-F, referred to as DDVF hereafter) to recruit members of the cellular p90-ribosomal S6 protein kinases (RSKs) family: RSK1, RSK2, RSK3 and RSK4 [1,2]. Interestingly, competition and cross-linking experiments, as well as crystallography data show that these pathogens' proteins, the leader (L) protein (cardioviruses), ORF45 (Kaposi sarcoma-associated herpes virus - KSHV) and YopM (*Yersinia*) use a common interface to recruit RSKs. Binding of the pathogens' proteins prevents RSK dephosphorylation by cellular phosphatases, thereby maintaining RSK

in an active state [1,2]. Although infection with all three pathogens leads to RSK activation, the outcome of this activation differs according to the protein bound to RSK. YopM association with RSK was proposed to inhibit the inflammasome and to lead to IL-10 production [3,4]; RSK recruitment by ORF45 enhances lytic replication of KSHV [5,6], whereas RSK recruitment by cardiovirus L protein leads to the inhibition of the antiviral eukaryotic initiation factor 2 alpha kinase 2 (EIF2AK2), better known as PKR [1].

PKR inhibition by L was shown to depend on L interaction with RSK but also on L protein's C-terminal domain. Indeed, the M60V mutation in the C-terminal domain of L does not affect RSK recruitment but abolishes PKR inhibition. These observations led us to propose the "model of the clamp" whereby pathogens' proteins would act as adaptor proteins that force a given enzyme (here RSKs) to act on a specific substrate. Through their DDVF motif, pathogens' proteins recruit and maintain RSKs in an activated state. Through another domain (i.e. the C-terminal domain for L), they recruit proteins that could serve as substrate for RSKs. After phosphorylation, such proteins would act as effectors to the benefit of the pathogen (Fig 1A) [1]. In an alternative model, proteins interacting with RSK through the conserved DDVF motif could directly act as preferential substrates for RSK-mediated phosphorylation (Fig 1B), as was suggested for the cellular protein RHBDF1 (Rhomboid 5 homolog 1) [2].

Cardioviruses belong to the *Picornaviridae* family and include encephalomyocarditis virus (EMCV), Theiler's murine encephalomyelitis virus (TMEV) and the human Saffold virus (SAFV), closely related to TMEV. Despite its very small size (67-76 amino acids) and lack of enzymatic activity, the L protein encoded by these viruses was shown to be multifunctional as, beside inhibiting PKR, it blocks interferon gene transcription, and triggers an extensive diffusion of nuclear and cytoplasmic proteins across the nuclear

membrane [1,7-16]. This nucleocytoplasmic trafficking perturbation was associated with the hyperphosphorylation of phenylalanine-glycine-nucleoporins (FG-NUPs) such as NUP98, NUP153 or NUP62 [17-20]. FG-NUPs are proteins of the nuclear pore complex (NPC) that possess intrinsically disordered domains, rich in phenylalanine and glycine residues. These domains form a mesh in the center of the nuclear pore, which enables interaction with karyopherins, thus allowing selective transport of proteins and RNA through the NPC [21-24]. Molecular dynamic simulations predict that FG-NUP phosphorylation drastically decreases the density of FG-NUPs inside the pore [25]. Accordingly, electron microscopy analysis of EMCV-infected cells displayed such a density loss in the center of the NPC [20]. Through perturbation of the NPC, cardioviruses trigger a diffusion of nuclear proteins to the cytoplasm which can be used by the virus for viral replication and translation [16].

Preliminary data suggested that nucleocytoplasmic trafficking perturbation by cardiovirus L proteins depended on RSK and on the recruitment of a cellular target by the L-RSK complex (model of the clamp). The aim of this work was to assess whether RSK could indeed be retargeted by L to a new substrate in infected cells and to identify such a substrate that could trigger nucleocytoplasmic trafficking perturbation. Our data show that L can recruit both RSK and FG-NUPs and that FG-NUPs can act as direct RSK substrates in infected cells. This work provides strong support to the model of the clamp and elucidates a novel virulence mechanism.

# Results

## Cardiovirus L-mediated nucleocytoplasmic trafficking perturbation depends on RSK recruitment by L

We tested whether L-mediated redistribution of nuclear and cytoplasmic proteins across the nuclear envelope and the hyperphosphorylation of FG-NUPs depends on both RSK and L. In agreement with previous reports [14], cytosolic diffusion of the nuclear protein PTB occurred in HeLa cells infected for 10 hours with TMEV expressing a wild type L protein ($L^{WT}$) but not in non-infected cells or in cells infected with viruses carrying the M60V mutation in the C-terminal part of L ($L^{M60V}$)(Figs 2A and B). In the latter cells, PTB however partly appeared in cytosolic punctae, likely corresponding to stress granules that were shown to form in the absence of PKR inhibition by L [12]. Importantly, $L^{WT}$-mediated PTB diffusion was almost abrogated in RSK-deficient HeLa cells (HeLa-RSK-TKO) (Figs 2B and C). Viral replication was also decreased in the absence of RSK, in agreement with increased PKR activation in these cells (Fig 2D). Interestingly, PTB diffusion was restored after transduction of HeLa-RSK-TKO cells with lentiviruses expressing any of the four human RSK isoforms (Figs 2B and C). Accordingly, NUP98 hyperphosphorylation was dramatically decreased in HeLa-RSK-TKO cells and restored in cells transduced to express any of the four RSK isoforms (Fig 2D). Similar observations were made in the case of EMCV as soon as 5 hours post-infection, although dependence on RSK was less pronounced (Figs 2E-H). Thus, PTB diffusion out of the nucleus and NUP98 hyperphosphorylation depend on both L and RSK.

In addition, TMEV and EMCV expressing $L^{WT}$ but not mutant L proteins triggered an RSK-dependent disruption of nucleocytoplasmic trafficking of other proteins harboring canonical

nuclear export (NES) and import (NLS) sequences, as shown by diffusion of GFP-NES and RFP-NLS proteins in live cells that stably express these proteins (Figs 3A-D). This observation demonstrates that nucleocytoplasmic redistribution of proteins was not specific to PTB. Again, RSK dependence of protein redistribution was slightly less prominent for EMCV than for TMEV.

Ectopic expression of TMEV $L^{WT}$ but not the $L^{F48A}$ mutant (affected in the RSK-binding motif) was sufficient to trigger nucleocytoplasmic redistribution of proteins (Figs 3E-G). Also, expression of $L^{M60V}$ or YopM did not affect nucleocytoplasmic trafficking although these proteins can activate RSK [1]. Taken together, these data show that L-mediated nucleocytoplasmic trafficking alteration does not dependent on virus replication per se or on the expression of other viral proteins and requires both interaction with RSK and, at least for TMEV L, integrity of the C-terminal part of the protein.

## Identifying RSK partners in TMEV-infected cells using BioID2

According to the model of the clamp, TMEV L would recruit RSK through its central DDVF motif and would recruit potential RSK substrates through its C-terminal domain. As suggested above, the M60V mutation of L would prevent the recruitment of such a target, without affecting RSK binding.

In order to identify target proteins that are recruited by L as potential RSK targets, we used the modified bacterial biotin ligase BioID2 (BioID) which, when fused to a protein of interest, allows promiscuous biotinylation of proximal proteins in the cell [26].

A BioID-RSK2 (BioID-RSK) fusion was constructed and expressed in RSK1/2-deficient HeLa cells (HeLa-RSK-DKO) by lentiviral transduction to identify RSK's potential partners during TMEV infection (Fig 4A). After testing that the BioID-RSK construct was activated (i.e. phosphorylated) in the presence of L in infected cells and able to rescue L activities such

as L-mediated PKR inhibition (Fig S1A), we performed biotinylation experiments in order to identify RSK partners in the context of infected cells. HeLa BioID-RSK cells were infected with either $L^{WT}$ or $L^{M60V}$ viruses for 16 hours in presence of biotin. Biotinylated proteins were pulled down using streptavidin beads and processed for mass spectrometry analysis. Western blot detection of biotinylated proteins (Fig 4B) confirmed the concentration of biotinylated proteins in the pulled down fraction and revealed the presence of a 100kDa band specific to the $L^{WT}$-infected sample, suggesting that the L protein status indeed influenced target biotinylation by the BioID-RSK fusion.

## Identifying L protein partners using BioID

Several attempts to identify proteins that are recruited by TMEV L were made in our lab by coimmunoprecipitation. However, beside RSK, no clear L partner was consistently identified. It is not unlikely that proteins recruited by L would interact with L only transiently and with low affinity. We thus used the BioID system to identify such proteins that may transiently interact with L in infected cells and then serve as RSK substrates. However, due to packaging limitations in picornaviruses, the BioID coding sequence (696 nt) would be too long to be accommodated into the viral genome. We thus generated *trans*-encapsidated replicons where a sequence coding for BioID-L and eGFP was substituted for the capsid-coding region (Fig 4C). These replicons were encapsidated in 293T cells stably expressing a capsid coding sequence carrying synonymous mutations in the VP2 region that affect *CRE* function [27] to prevents the selection of replication-competent wild type viruses that might emerge through recombination. *Trans*-encapsidated replicons coding for BioID fused to $L^{WT}$, $L^{M60V}$ and $L^{F48A}$ were produced (Fig 4A). In HeLa cells infected with these replicons, L activities (i.e. RSK phosphorylation, PKR activation and NUP98 hyperphosphorylation) were as expected (Fig S1B). HeLa cells were then infected with BioID-L replicons for 14 hours in presence of

biotin. Biotinylated proteins were pulled down in stringent conditions. Western blot confirmed protein biotinylation in infected cell extracts and showed some bands occurring in $L^{WT}$ and $L^{F48A}$ but not in $L^{M60V}$ samples (Fig 4D). These results confirm specific biotinylation of proteins by BioID-L.

## FG-NUPs are enriched in BioID-L and BioID-RSK proxeomes

We expected that RSK targets recruited by L would be present in both BioID-RSK and BioID-L screens. Pulled down biotinylated proteins from both screens (n=3 for each screen) were identified by mass spectrometry (MS) and sorted according to their peptide spectrum match (PSM) number (for more detail on the calculations see material and methods). For BioID-RSK, proteins were sorted according to their abundance in $L^{WT}$-infected cells relative to that in non-infected cells and in cells infected with the $L^{M60V}$ mutant virus (Fig 5A, vertical axis). For BioID-L (replicons), proteins were sorted according to their abundance in $L^{WT}$ and $L^{F48A}$ samples relative to that in $L^{M60V}$-infected and in non-infected samples (Fig 5A, horizontal axis). Hence, the proteins that would be recruited by the C-terminal domain of L are those that have high ratios in both screens. Interestingly, many of these proteins were FG-NUPs (Figs 5A and B). ProDA (Probabilistic Dropout Analysis) statistical analysis [28] was used to identify proteins whose abundance differs in pairwise comparisons: $L^{WT}$ versus $L^{M60V}$ for the BioID-RSK experiments, and $L^{WT}$ versus $L^{M60V}$ or $L^{F48A}$ versus $L^{M60V}$ for the BioID-L experiment. The table in Fig 5B shows adjusted P-values obtained from this analysis for the 20 best-ranked proteins. In the BioID-RSK experiments, FG-NUPs had the lowest adjusted P-values (though not significant) and highest fold change (Figs 5B and C). In the BioID-L experiments many FG-NUPs reached significant scores when pairwise comparisons were made between $L^{WT}$ and $L^{M60V}$ or between $L^{F48A}$ and $L^{M60V}$ (Figs 5B and C). Most importantly, FG-NUPs that had previously been shown to be hyperphosphorylated during

188 cardiovirus infection: NUP62, NUP98, NUP153 and NUP214 [17-20] exhibited statistical
189 significance (Fig 5B). From these results we conclude that L recruits RSK through its DDVF
190 motif and then docks RSK toward FG-NUPs when the C-terminal domain of L is intact.
191

192 **Proteins biotinylated by BioID-RSK and BioID-L are localized at the NPC**

193 We analyzed the subcellular localization of proteins that were biotinylated by BioID-RSK
194 and by BioID-L in infected cells. To this end, biotinylation experiments were performed as
195 above but infected cells were fixed after 10h of infection, permeabilized and stained them
196 with Alexa Fluor conjugated streptavidin. For BioID-RSK, mock-infected cells show staining
197 of biotinylated proteins in the nucleus, in agreement with the mostly nuclear localization of
198 RSKs [29] (Figs 6A-C). In cells infected with the $L^{WT}$ virus, biotinylated proteins form a faint
199 rim around the nucleus that colocalizes with the FG-NUP NUP98, in addition to the diffuse
200 nuclear staining, showing that part of the (BioID)-RSK molecules are recruited to the nuclear
201 envelope. In cells infected with the $L^{M60V}$ mutant virus, this nuclear rim is lost, in agreement
202 with a lack of $L^{M60V}$ interaction with nucleoporins.
203

204 For BioID-L replicons, staining occurs in the nucleus and at the nuclear envelope for $L^{WT}$, in
205 agreement with an interaction of L with both RSK and NUPs (Figs 7A-C). Proteins
206 biotinylated by BioID-$L^{M60V}$ show diffuse staining in the nucleus, in agreement with $L^{M60V}$
207 interaction with RSK but not with nucleoporins. Proteins biotinylated by BioID-$L^{F48A}$ show
208 extensive colocalization with nucleoporin POM121 at the nuclear envelope (Fig 7C), in
209 agreement with the lack of interaction with RSK, which would likely sequester part of the L
210 protein in the nucleoplasm. In conclusion, labeling of biotinylated proteins support our model
211 where L interacts with RSK in the nucleus and recruits a portion of RSK molecules to the
212 NPC, via an interaction between the C-terminal domain of L and NUPs.

## FG-NUPs are direct substrates for RSK in cardiovirus infected cells

Since FG-NUPs are known to be hyperphosphorylated during cardiovirus infection and since our results showed that RSK is in their close proximity, we aimed to test if RSK can directly phosphorylate these FG-NUPs in infected cells. For this, we used the « analog-sensitive kinase system » developed by the group of Shokat [30]. This system is based on the use of an ATP analog: N6-alkylated ATP-γ-S (A*TP-S), bulkier than ATP, that only fits in ATP binding pockets of kinases that have been mutated to accommodate such bulkier analogs. The advantage of this technique is that the mutated kinase (RSK in our case) is the only kinase in the cell that can use A*TP-S and will therefore thiophosphorylate its substrates. After alkylation, such target proteins can be recognized using a specific anti-thiophosphate ester antibody (Fig 8A). We identified Leu147 as the RSK2 gatekeeper residue (i.e. residue in the ATP-binding pocket that, when mutated to a smaller residue, allows the access of the A*TP-S) by homology to Thr338 in the consensus sequence defined for c-SRC [31] (Fig 8B). Leu147 was mutated either to Gly (As1-RSK) or to Ala (As2-RSK). To test for ATP analog usage by the modified RSK kinases, WT, As1- and As2-RSKs were stably expressed in HeLa-RSK-TKO cells by lentiviral transduction, yielding WT-, As1- and As2-RSK cells. Expression of both As1- and As2-RSK allowed L functions (i.e. PKR inhibition, RSK activation and NUP98 hyperphosphorylation) (Fig S2A). The ATP analog N6-Bn-ATP-γ-S was better incorporated than N6-PhEt-ATP-γ-S by the As-RSKs (Fig S2B). The As2-RSK kinase was better expressed than As1-RSK and readily accommodated this analog (Figs S2A and B). Therefore, As2-RSK cells and N6-Bn-ATP-γ-S were chosen for further experiments. HeLa WT-RSK or As2-RSK cells were then infected with $L^{WT}$ and $L^{M60V}$ viruses for 8h30min. Cells were then permeabilized with digitonin and treated with A*TP-S (N6-Bn-ATP-γ-S) for 1 hour. Then, NUP98 was immunoprecipitated and its thiophosphorylation status was

238 analyzed, after alkylation, by western blot with the anti-thiophosphate ester antibody. The
239 blot shown in Fig 8C shows a band highly enriched in the immunoprecipitated sample,
240 migrating at the expected molecular mass for NUP98 (98kDa). This band was most
241 prominent in the samples from As2-RSK cells, confirming the specificity of thiophosphate
242 ester detection. Importantly, this band was detected much more in samples of cells infected
243 with the $L^{WT}$ virus than in samples of cells that were not infected or infected with the $L^{M60V}$
244 virus. These data indicate that NUP98 can be directly phosphorylated by RSK and that, as
245 expected, this phosphorylation only occurs after infection with the $L^{WT}$ virus. For EMCV, as
246 this virus replicates much faster than TMEV, NUP98 was immunoprecipitated after 3h30 of
247 infection. Thiophosphorylation of immunoprecipitated proteins was tested by western blot
248 using the anti-thiophosphate ester antibody (Fig 8D). As for TMEV, a ~100kDa protein likely
249 corresponding to NUP98 was thiophosphorylated by As2-RSK only in $L^{WT}$ infected
250 conditions. It is noteworthy that additional bands were detected, which likely correspond to
251 other FG-NUPs such as NUP62, NUP153 and NUP214 that coimmunoprecipitated with
252 NUP98.
253 In order to confirm FG-NUPs thiophosphorylation by As2-RSK in infected cells, experiments
254 were performed the other way around. Therefore, thiophosphorylated proteins were
255 immunoprecipitated from cells infected with TMEV variants, using the thiophosphate ester
256 antibody. Then the IP fraction (i.e. thiophosphorylated proteins) was analyzed by western
257 blot for the presence of NUP98 (Fig 8E) and NUP214 (Fig S2C). Again, these NUPs were
258 most prominently detected in the conditions where the L protein was WT and RSK was
259 mutated (As2-RSK). These data confirm that RSK directly phosphorylates FG-NUPs when
260 the $L^{WT}$ protein is present.
261

Taken together, these results confirm that part of the cellular RSKs can be redirected to the nuclear pore complex by the L protein, where RSKs phosphorylate FG-NUPs. By interacting with RSK through its DDVF motif and with FG-NUPs through its C-terminal domain, L serves as a viral adapter protein to modulate RSK's activity and redirects these kinases toward new substrates thus supporting the model of the clamp. Hyperphosphorylation of FG-NUPs by RSK likely triggers a global perturbation of nucleocytoplasmic trafficking and may therefore facilitate cytoplasmic replication of cardioviruses.

# Discussion

Recent work showed that some proteins expressed by unrelated viruses and bacteria hijack host RSK kinases through a conserved DDVF linear motif that likely emerged in those proteins by convergent evolution [1,2]. Occurrence of the DDVF motif in RHBDF1, a known target of RSKs suggests that some proteins, either from pathogens or from the host cell, can associate with RSK through the DDVF motif to promote their own phosphorylation by RSKs [2]. In the case of TMEV L protein, a point mutation in the C-terminal domain of the protein ($L^{M60V}$) abrogated L activities although this mutation affected neither L-RSK interaction nor RSK activation by L [1,32]. The phenotype of this mutant supported the model of the clamp where the pathogens' protein would act to bridge RSK to specific substrates. The two models are not mutually exclusive.

Our data show that L proteins from TMEV and EMCV indeed act by redirecting part of the cellular RSK kinases toward the nuclear pore complex where RSKs directly phosphorylate FG-NUPs.

Bacteria of the genus *Yersinia* use a type III secretion system to inject Yop proteins into contacted eukaryotic cells [33]. YopM was shown to interact with RSK through a C-terminal

DDVF motif [1] and with protein kinase PKNs through central leucin-rich motifs. Formation of the tripartite (YopM-RSK-PKN) complex results in the phosphorylation and activation of PKN, which requires active RSK [34,35], suggesting that RSK might also be redirected toward PKN as a specific substrate. This scenario is very likely although direct phosphorylation of PKN by RSK was not formally proven.

Another question regarding the clamp model is whether the substrates to which RSKs are redirected by the pathogens' proteins are physiological RSK substrates, the phosphorylation of which is increased by their forced association with RSKs or whether they represent unconventional RSK substrates. From the blots of analog-sensitive RSK experiments (Figs 8C-E and S2C), it appears that basal thiophosphorylation of NUP98 or NUP214 might occur, even in non-infected cells that do not contain the L protein. Also, given that the main binding site of pathogens' proteins is located in a surface-exposed loop of RSK, relatively remote from the catalytic site, it is unlikely that this interaction can modify the catalytic site enough to accommodate structurally divergent substrates. Thus, the role of the bridging proteins is likely to increase the frequency of encounters between RSKs and specific substrates, and possibly also to drive these kinases to specific subcellular locations.

Viruses of the *Picornaviridae* family disturb nucleocytoplasmic traffic, likely to recruit host nuclear RNA-binding proteins to the cytoplasm of the infected cells, where their genome translation and replication takes place. Perturbation of the traffic was also reported to inhibit the activation of innate immunity genes such as genes coding for interferon or chemokines, because these genes rely on the translocation of transcription factors like IRF3/7 or NFκB [16,36]. Enteroviruses encode proteases $2A^{pro}$ and $3C^{pro}$, which directly cleave FG-NUPs [37], thereby opening the central channel of the nuclear pore complex [20,38]. Cardioviruses, however, induce the hyperphosphorylation of FG-NUPs, thus mimicking a process occurring during mitosis, which ends up in the dismantling of the NPCs and the free diffusion of

311 nuclear and cytoplasmic proteins. Here, we show that TMEV L promotes direct FG-NUPs
312 phosphorylation by RSKs. During mitosis, FG-NUP phosphorylation was proposed to
313 involve mostly cyclin-dependent kinase 1 (CDK1), polo-like kinase 1 (PLK1) and NIMA-
314 related kinases [23,39]. A phosphoproteomic analysis by Kosako et al. [40] also suggested the
315 involvement of the ERK pathway, ERK1/2 being the upstream kinase of RSK. We
316 hypothesize that RSKs might indeed contribute, to some extent, to NUP phosphorylation
317 during mitosis and that L triggers a stronger RSK-mediated FG-NUP phosphorylation during
318 infection.
319 Our work illustrates a new virulence mechanism whereby pathogens' proteins not only
320 activate but also redirect host kinases toward specific substrates and decipher how
321 cardioviruses trigger RSK-mediated FG-NUP hyperphosphorylation to perturb
322 nucleocytoplasmic trafficking in the host cell.
323

# 324 Material & methods

325

326 **Cells**

327 The subclone of HeLa cells used in this work were HeLa M cells kindly offered by R.H.
328 Silvermann [41].
329 HeLa-RSK-DKO, (RSK1- and RSK2-deficient) and HeLa-RSK-TKO (RSK-1, RSK2- and
330 RSK3-deficient) cells were obtained from HeLa M cells using the CRISPR-Cas9 technology
331 [1]. HeLa-LVX and HeLa-RSK-TKO-LVX were obtained by transduction of HeLa M cells and
332 of HeLa-RSK-TKO cells with pLVX-EF1alpha-2xGFP:NES-IRES-2xRFP:NLS. Clones
333 showing regular 2xGFP:NES and 2xRFP:NLS expression levels under the fluorescent
334 microscope were selected for further use. HeLa BioID-RSK cells were obtained by

transduction of HeLa-RSK-DKO cells with BLP10 and transduced cell populations were then selected with 1mg/ml of G418 (Roche). HeLa WT-RSK, HeLa As1-RSK and HeLa As2-RSK cells were obtained by transduction of HeLa-RSK-TKO cells with TM1117, BLP20 and BLP21 respectively and transduced cell populations were selected with 1mg/ml of G418 (Roche).

HeLa-RSK-TKO cells were transduced with the empty lentiviral vector TM952 or with TM1116-19 derivatives expressing the four isoforms of human RSK. Transduced cell populations were selected with 2mg/ml of G418.

BHK-CL13 and 293T-CL13 cells were obtained by lentiviral transduction of CL13. mCherry-positive cells were then sorted by FACS.

293T cells were kindly provided by F. Tangy (Pasteur Institute, Paris). Both HeLa M and 293T cells and their derivatives were maintained in Dulbecco's modified Eagle medium (DMEM) (Lonza) supplemented with 10% of fetal calf serum (FBS, Sigma), 100 U/ml penicillin and 100µg/ml streptomycin (Thermo Fisher). BHK-21 cells (ATCC), were maintained in Glasgow's modified Eagle medium (GMEM) (Gibco) supplemented with 10% newborn calf serum (Gibco), 100 U/ml penicillin, 100µg/ml streptomycin and 2.6g/l tryptose phosphate broth (Difco). All cells were cultured at 37°C, in 5% CO2.

**Viruses**

TMEV viruses used in this study are derivatives of KJ6, a variant of the persistent DA strain (DA1 molecular clone) adapted to grow on L929 cells [42]. FB09 carries the M60V mutation in L ($L^{M60V}$), which was shown to abrogate L toxicity [12,32]. KJ6 and FB09 are indicated as TMEV $L^{WT}$ and $L^{M60V}$ respectively.

EMCV viruses used is this study are derived from pMC24 , a Mengo virus molecular clone carrying a shortened (24C) polyC tract [43]. The virus denoted $EMCV^{WT}$ (used in Fig 8) is the

360 virus produced from the pMC24 plasmid. Viruses denoted EMCV $L^{WT}$ and $L^{Zn}$ (used in Figs
361 2 and 3) are produced from plasmids pFS269 and pTM1098 and express N-terminally Flag-
362 tagged L proteins. $L^{Zn}$ carries two point mutations (C19A and C22A) in the zinc finger of L,
363 which likely affect the overall structure of the protein [44].
364 These viruses were produced by reverse genetics from plasmid constructions containing the
365 full-length viral cDNA sequences. To this end, BHK-21 cells were electroporated (1500V,
366 25µFd, no shunt resistance) using a Gene pulser apparatus (Bio-Rad) with viral RNA
367 produced by *in vitro* transcription (RiboMax P1300, Promega). Supernatants were collected
368 48-72h after electroporation, when cytopathic effect was complete. After 2 to 3 freeze-thaw
369 cycles, the supernatants containing the virus were clarified by centrifugation at 1258g for 20
370 min and viruses were stored at -80°C. Viruses were titrated by plaque assay in BHK-21 cells.
371
372 **Trans-encapsidated viral replicons**
373 FW12 is the replicon encoding for BioID2-HA-linker(3xGGGGS)-$L^{WT}$. This replicon derives
374 from TMEV DA1. It was constructed by replacing the capsid-coding region of the virus by a
375 sequence coding sequentially (5'-to-3'), in a single frame, for: BioID2-HA-
376 linker(3xGGGGS)-L, the L/VP4 boundary cleaved by protease 3C, eGFP, the VP2 coding
377 segment encompassing the CRE sequence, the 3' end of the 2A coding region and the
378 following part of the viral genome (see Fig 4). The BioID-$L^{M60V}$ (FW16) and BioID-$L^{F48A}$
379 (FW17) viral replicons are derivates of FW12 carrying the indicated mutation. Trans-
380 encapsidation of the replicon occurred in 293T-CL13 to stably express the viral capsid
381 precursor protein. C-terminal residues of L were inserted in the construct to restore a genuine
382 L/VP4 clivage site for protease 3C, which allows the capsid protein to start with an N-
383 terminal glycine, potentially undergoing myristoylation [45]. Importantly, 4 silent mutations
384 were introduced in the VP2 coding sequence corresponding to the *CRE* region to prevent the

385 replication of recombinant wild type viruses that would emerge through recombination
386 between replicon RNA and capsid-coding mRNA in packaging cells.
387 293T-CL13 cells were seeded (600,000/well) in 6-well plates. 24h after seeding, cells were
388 transfected (TransIT-mRNA, Mirus) with 5µg of replicon RNA previously obtained by *in*
389 *vitro* transcription. Six hours post-transfection, medium was changed to DMEM without
390 serum. The infected cells were passaged 8 times and reseeded with part of the collected
391 supernatant to amplify viral production. Then, 150ml of replicon-containing supernatant was
392 collected and filtered (0.45µm). SDS was then added to a final concentration of 0.5% and,
393 after 2h incubation at RT, supernatants were centrifuged for 5min, at 1258g at 20°C. Next,
394 13ml of clarified supernatant was added to a 2.6ml sucrose 30% cushion in polyallomer tubes
395 (Beckman) and centrifuged for 16h at 20°C, 25000rpm in a SW28 swinging bucket rotor.
396 After ultracentrifugation, pellets containing the replicons were resuspended in 150µl of
397 10mM Tris-HCl pH 7.5 and further dialyzed in 10mM Tris-HCl pH 7.5. Replicons were then
398 titrated by plaque assay using BHK-21 cells stably expressing viral capsid proteins (BHK-21
399 CL13), and kept at -80°C.
400
401 **Lentiviral vectors and cell transduction**
402 - pLVX-EF1alpha-2xGFP:NES-IRES-2xRFP:NLS was a gift from Fred Gage (Addgene
403 plasmid # 71396) [46]
404 Other lentiviral vectors used for protein expression were derived from
405 pCCLsin.PPT.hPGK.GFP.pre. [47]
406 - TM945 is a $Prom_{CMV}$-MCS-IRES-mCherry construct [48]
407 - TM952 is a $Prom_{CMV}$-MCS-IRES-neo construct [49]
408 - BLP10 is a TM952 derivative coding for BioID2-HA-linker(3xGGGS)-MuRSK2. This
409 construct expresses murine RSK2, which differs from human RSK2 by a single amino acid.

- BLP20 is a TM952 derivative coding for As1-RSK2 (hu-RSK2 with Analog-sensitive kinase 1 (As1) mutation (Leu 147 → Gly ).
- BLP21 is a TM952 derivative coding for As2-RSK2 (hu-RSK2 with Analog-sensitive kinase 2 (As2) mutation (Leu 147 → Ala ).
- CL13 is a TM945 derivative expressing the 10 C-terminal aminoacids of L followed by the entire capsid precursor of virus DA1.
- TM1116, TM1117, TM1118 and TM1119 are TM952 derivatives carrying the sequences coding for 3xHA-Human RSK1, RSK2, RSK3 and RSK4 respectively [1]. They were constructed using the Gateway technology (Invitrogen) from donor plasmids Hs.RPS6KA1, Hs.RPS6KA2, Hs.RPS6KA3 and Hs.RPS6KA6 kindly provided by Dominic Esposito through the Addgene collection (Addgene refs: 70573, 70575, 70577, and 70579, respectively)

Lentiviruses were produced in 293T cells by co-transfection of the following plasmid, using TransIT-LT1 reagent (Mirus Bio): 2.5 µg of lentiviral vector, 0.75 µg of pMD2-VSV-G (VSV-glycoprotein), 1.125 µg of pMDLg/pRRE (Gag-Pol), and 0.625 µg of pRSV-Rev (Rev). DNA quantities are for transfection of 1 well of a 6-well plate. Supernatants were typically collected 72h post transfection and filtered (porosity: 0.45µM). For transduction, cells were typically seeded in a 24-well plate as of 5,000 - 10,000 cells/well and infected 1 or 2 times with 100µL of filtered lentivirus.

**Biotinylation experiments**

BioID-RSK : HeLa BioID-RSK cells were seeded in 6-well plates at a density of 90,000 cells per well. Two 6-well plates were used per condition. 24h after seeding the cells, the medium was changed to OptiMEM (Gibco) depleted from biotin (previously incubated with streptavidin beads for 2h at 4°C, then filtered). Cells were kept in OptiMEM without biotin

for 48h, then they were infected with 600µl of virus per well at an MOI of 2.5. One hour post-infection 2ml/well of DMEM containing 5µM biotin was added. Infection proceeded for 16h. For immunostaining, same protocol with these differences: 1,000 HeLa BioID-RSK cells were seeded in wells of a 96-well plate. Cells were infected with 50µL of virus per well at an MOI of 5 and infection proceeded for 10h.

BioID-L : HeLa cells were seeded in 6-well plates as of 160,000 cells per well. Two 6-well plates were used per condition. 24h after seeding, the cells were infected with 600µl of BioID-L replicons at an MOI of 2.5. One hour post-infection 2ml/well of DMEM containing 5µM biotin was added. Infection proceeded for 14h. For immunostaining, same protocol with these differences: 3,500 HeLa cells were seeded in wells of a 96-well plate. Cells were infected with 50µL of virus per well at an MOI of 5 and infection proceeded for 10h.

**Streptavidin Pulldown**

Cells were washed with PBS 3 times and lysed with 200µL/well of stringent lysis buffer (50mM Tris-HCl pH 7.6, 500mM NaCl, 0.4% SDS, 1mM DTT, 1 tablet of Pierce phosphatase/protease inhibitor (Thermo Scientific) per 10ml of lysis buffer) for 15 min at room temperature (RT). Lysates were then diluted twice by addition of 200µl/well of 50mM Tris-HCl pH7.6 and homogenized by 10 passages through 21G needles. Lysates were then cleared by centrifugation at 12,000g for 10 min at RT. Supernatants were transferred to new tubes, 200µL (per condition) of protein A/G magnetic beads (Pierce) were added to remove non-specific binding and incubated for 30 min at RT. Supernatants were then transferred to a new tube and a sample of 160µL per condition was mixed with 80µL of 3x Laemmli buffer (cell lysate control). The rest of the supernatant was incubated for 2h at RT with 260µL (per condition) of Streptavidin magnetic beads (Pierce). Streptavidin beads were then washed once with 2% SDS, and twice with “normal lysis buffer” (50mM Tris-HCl pH 7.5, 100mM

460 NaCl, 2mM EDTA, 0.5% NP40, 1 tablet of phosphatase/protease inhibitor (Thermo
461 Scientific) per 10ml of lysis buffer) for 5 min at RT. Beads were resuspended in 40µl of 1x
462 Laemmli buffer and heated for 5min at 100°C to allow protein's separation from the beads.
463 Supernatants were then conserved at -20°C.
464

465 **Immunostaining**

466 Immunostaining was performed as described previously [49]

| **Antibody** | **Dilution** | **Reference** |
|---|---|---|
| Anti-TMEV 3D polymerase (rabbit) | 1/1000 | kindly provided by M.Brahic |
| Anti-2A (rabbit) | 1/1200 | Home-made |
| Anti-NUP98 (rat) | 1/400 | N1038 - Sigma |
| Anti-POM121 (rabbit) | 1/400 | 15645-1-AP - Proteintech |
| Anti-PTB (mouse) | 1/400 | 324800 - Invitrogen |
| | | |
| Anti-rabbit Alexa Fluor 594 (chicken) | 1/800 | A21442 - Molecular Probes |
| Anti-rabbit Alexa Fluor 488 (Goat) | 1/800 | A11008 - Molecular Probes |
| Anti-rat Alexa Fluor 594 (chicken) | 1/800 | A21471 - Molecular Probes |
| Anti-mouse Alexa Fluor 488 (Goat) | 1/400 | A11029 - Molecular Probes |
| Streptavidin Alexa Fluor 488 | 1/500 | S32354 - Invitrogen |
| Streptavidin Alexa Fluor 594 | 1/500 | S32356 - Invitrogen |

467

468 **Western blotting**

469 Western blots were performed as described previously [49]

| **Antibody** | **Dilution** | **Reference** |
|---|---|---|

| | | |
|---|---|---|
| Anti-2A (rabbit) | 1/4000 | Home-made |
| Anti-Phospho-S380-RSK (rabbit) | 1/4000 | CST11989 |
| anti-PKR (rabbit) | 1/4000 | 18244-1-AP |
| anti-Phospho-T446-PKR (rabbit) | 1/4000 | AB32036 |
| anti-ß-actin (mouse) | 1/10000 | A5441- Sigma |
| anti-TMEV 3D polymerase (rabbit) | 1/2000 | kindly provided by M.Brahic |
| anti-NUP98 (rat) | 1/2000 | N1038 - Sigma |
| anti-HA (mouse) | 1/4000 | MMS101P - Covance |
| anti-phospho-Akt/RSK-substrates:RxxS*/T* (rabbit) | 1/1000 | CST9614 |
| anti-thio-P-ester (rabbit) | 1/1000 | NBP2-67738 |
| anti-TMEV capsid (mouse) | 1/2000 | Home-made |
| anti-FLAG M2 | 1/5000 | F1804 - Sigma |
| | | |
| Anti-rabbit-HRP (Goat) | 1/5000 | P0448 – Dako |
| Anti-mouse-HRP (Goat) | 1/5000 | P0447 – Dako |
| Anti-rat-HRP (Rabbit) | 1/5000 | P0162 – Dako |
| Streptavidin-HRP | 1/5000 | P0397 – Dako |

470

471

472 **Mass spectrometry**

473 Mass spectometry analysis was performed as described previously [50,51]. Streptavidin
474 pulldown samples were resolved using a 10% Tris-Glycine SDS gel run until 6mm migration
475 in the separating gel. Proteins were colored using PageBlue (Thermo Scientific, 24620). The
476 6mm bands containing whole proteins were cut into 3 different slices and trypsin digested (50

ng/µl in 50 mM NH4HCO3 buffer, pH 8.0). The peptides were analyzed by capillary LC-tandem mass spectrometry using an Orbitrap Fusion Lumos tribrid ion trap mass spectrometer (ThermoFisher Scientific). The resulting MS/MS data was processed using Sequest HT search engine within Proteome Discoverer 2.5 SP1 against a *Homo Sapiens* protein database obtained from Uniprot (78 787 entries) and containing the sequences of viral proteins and BioID2-RSK. Trypsin was specified as cleavage enzyme allowing up to 2 missed cleavages, 4 modifications per peptide and up to 5 charges. Mass error was set to 10 ppm for precursor ions and 0.1 Da for fragment ions. Oxidation on Met (+15.995 Da), phosphorylation on Ser, Thr and Tyr (+79.966 Da), conversion of Gln (-17.027 Da) or Glu (-18.011 Da) to pyro-Glu at the peptide N-term, biotinylation of Lys (+ 226.077) were considered as variable modifications. False discovery rate (FDR) was assessed using Percolator and thresholds for protein, peptide and modification site were specified at 1%. PSM Ratio calculations were as followed:

$$BioID-RSK: \frac{PSM(L^{WT})}{PSM(L^{M60V})+PSM(mock)+1} \qquad BioID-L: \frac{PSM(L^{WT})+PSM(L^{F48A})}{PSM(L^{M60V})+PSM(mock)+1}$$

**_In vitro_ kinase assay**

293T cells were seeded (500,000 cells/well) in 6-well plates. 24h after seeding, cells were transfected with TransIT-LT1 reagent (Mirus Bio) with 2.5 µg of plasmids pTM1117, pBLP20 and pBLP21. 6 hours post-transfection, cells were treated with 32nM PMA over-night. HA-RSKs were then immunoprecipitated with anti-HA magnetic beads and resuspended in 30µl of TBS, 1mM PMSF, 1mM $Na_3VO_4$, 1 tablet of phosphatase/protease inhibitor (Thermo Scientific) per 10ml.

For one *in vitro* kinase reaction we put: 2.5µg of GST-S6 (recombinant substrate), 10µL of kinase buffer 5x (125mM Hepes pH 7.5, 250mM NaCl, 100mM ß-glycerophosphate, 5mM DTT, 100mM $MgCl_2$, 500µM $Na_3VO_4$), 0.5 µL of 10mM ATP (Roth, HN35.1) or A*TP

analogs (BioLog), and water to a final volume of 30µL. To this we added 10µL of the immunoprecipitated RSK and incubated everything at 30°C for 30 min with shacking. Following this, the samples were alkylated with PNBM (Abcam) at a final concentration of 2.5mM for 2 hours at room temperature with shacking. Reaction was stopped by the addition of Laemmli buffer 3x. Samples were then heated at 100°C for 5 min, separated from the magnetic beads and kept at -20°C.

**Thiophosphorylation in permeabilized cells**

1.5 x$10^6$ HeLa-RSK-TKO TM1117 or BLP21 cells were seeded in 10-cm dishes, 1 dish per condition. The next day, cells were infected at an MOI of 5 for 8h30min (for TMEV) and 3h30min (for EMCV). After that, cells were permeabilized with 500µL of the analog-kinase buffer: 20mM Hepes pH 7.5, 100mM KOAc, 5mM NaOAc, 2mM $MgOAc_2$, 1mM EGTA, 20µg/ml digitonin, 10mM $MgCl_2$, 0.5mM DTT, 1x phosphatase inhibitor cocktail 2 (P5726, Merck), 1x cOmplete protease inhibitor (REF), 57µg/ml creatin kinase (Calbiochem 23895), 5mM Creatin phosphate (Calbiochem, 2380), 0.1mM ATP, 0.1 mM N6-Bn-A*TP analog (BioLog), 3mM GTP (Roth, K056.4) in order to get the ATP analog inside the cells and the thiophosphorylation reaction to happen. Reaction proceeded for 1h at 37°C, 5% CO2 with the dishes on a rocking plate.

**Immunoprecipitation after thiophosphorylation reactions.**

NUP98 IP: cells were lysed by adding 500µL of 2x salty lysis buffer (100mM Tris-HCl pH8, 800mM NaCl, 2% Triton X-100, 4mM EDTA, 2mM DTT, 1 tablet of phosphatase/protease inhibitor (Thermo Scientific) per 10ml of lysis buffer) to the analog-kinase buffer for 15 min at 4°C. Lysates were diluted 4x by addition of 3ml of regular lysis buffer (50mM Tris-HCl pH8, 100mM NaCl, 0.5% NP40, 2mM EDTA, 1 tablet of phosphatase/protease inhibitor

(Thermo Scientific) per 10ml of lysis buffer). Lysates were then homogenized by 10 passages through 21G needles and cleared by centrifugation at 12,000g for 10min at 4°C. Supernatants were then transferred to new tubes, 30µL (per condition) of protein A/G magnetic beads (Pierce) were added to remove non-specific binding and incubated for 30 min at 4°C. Supernatants were then transferred to a new tube and a sample of 200µL/ condition was alkylated with PNBM at a final concentration of 2.5mM for 2h at RT.Alkylation reaction was stopped by addition of 3x Laemmli buffer (cell lysate control). The rest of the supernatant was incubated O/N at 4°C with 8µg (per condition) of anti- NUP98 (rat, N1038 – Sigma). 62.5µl of A/G beads per condition were added and incubated for 2h at 4°C. A/G beads were then washed three times with regular lysis buffer for 5 min at 4°C. Beads were resuspended in 40µl of kinase buffer 1x. The IP samples were then alkylated with PNBM at a final concentration of 2.5mM for 2h at RT. Alkylation reaction was stopped by the addition of 3x Laemmli, and immunoprecipitated proteins were separated from the beads after heating 5min at 100°C.

Thiophosphate ester IP: cells were lysed by adding 500µL of 2x lysis buffer (100mM Tris-HCl pH8, 200mM NaCl, 1% NP40, 40mM EDTA, 1 tablet of phosphatase/protease inhibitor (Thermo Scientific) per 10ml of lysis buffer) for 15min at 4°C. Lysates were then homogenized by 10 passages through 21G needles and cleared by centrifugation at 12,000g for 10min at 4°C. Supernatants were then alkylated with PNBM at a final concentration of 2.5mM for 1h30min at RT. As PNBM inhibits immunoprecipitation, lysates were run through PD10 columns to remove PNBM prior to the immunoprecipitation procedure. Fractions containing protein were kept and incubated with 30µl per condition of A/G magnetic beads (to avoid non-specific binding) for 30 min at 4°C. Supernatants were then transferred to a new tube and 1/10th of the lysate (200µl) was mixed with 100µl of 3x Laemmli (cell lysate control). The rest of the supernatant was incubated with 8µg per condition of anti-

thiophosphate ester antibody (rabbit, NBP2-67738 – Novusbio) for 2h at 4°C. Then 62.5µl per condition of A/G magnetic beads were added and incubated for 2h at 4°C. A/G beads were then washed three times with regular lysis buffer for 5 min at 4°C and resuspended in 60µl of Laemmli 1x. Immunoprecipitated proteins were separated from the beads after heating 5min at 100°C.

**Data processing and statistical analysis (for MS)**

Protein identification and label-free quantitation were performed with MaxQuant version 1.6.7.0.[52]. Database searching was performed against the UniProt FASTA database, using a false-discovery rate at the peptide and protein level was set to 0.01 and allowing a maximum of two missed cleavages. All search parameters are available in the parameter file available in the study repository (https://github.com/UCLouvain-CBIO/2022-RSK-Nups-VIRO). After filtering out of identified contaminants, identified reverse sequences and proteins having missing values in all samples, Max Quant protein intensities were log-2 transformed and normalized using sample median alignment. In order to cope with the numerous drop-outs in protein intensities, the proDA method, as described in [28] was applied.

For the analysis of the BioID-L experiment, the backbone linear model included one indicator variable representing a potential batch effect between 2 groups of replicates, and 2 condition indicator variables, representing the effect of resp. WT and F48A conditions with respect to the reference condition, i.e. M60V condition. Potential batch effect was tested for each protein using two-sided Wald test on the batch indicator variable. Since adjusted p-values were > 0.2 for all proteins, this indicator variable was subsequently removed from the model. Then, the effects of WT and F48 conditions (w.r.t. M60V) were tested, for each protein, using one-sided Wald tests, since the anticipated sign of the effect was known. All p-values were adjusted using Benjamini-Hochberg corrections [53].

For the analysis of the BioID-RSK experiment, the backbone linear model included one indicator variable representing a potential batch effect between 2 groups of replicates, and 1 condition indicator variable, representing the effect of WT condition with respect to the reference condition, i.e. M60V condition. Potential batch effect was tested for each protein using two-sided Wald test on the batch indicator variable. Since adjusted p-values were > 0.6 for all proteins, this indicator variable was subsequently removed from the model. Then, the effect of WT condition (w.r.t. M60V) was tested, for each protein, using a one-sided Wald test, since the anticipated sign of the effect was known. All p-values were adjusted using Benjaminin-Hochberg corrections.

**Statistical analysis on immunofluorescence**

Statistical analysis on immunofluorescence experiments was done using GraphPad Prism v9 A one-way ANOVA test was used. The number of independent experiments (n) and statistical comparison groups are indicated in the Figures and Figure legends.

**Materials & Correspondence**

Further information and requests for resources and reagents should be directed to and will be fulfilled by the lead contact, Thomas Michiels (thomas.michiels@uclouvain.be). All reagents generated in this study are available upon request after completion of a Materials Transfer Agreement

**Data and code availability**

The mass spectrometry proteomics data have been deposited to the ProteomeXchange Consortium via the PRIDE partner repository with the dataset identifier PXD034604".

MaxQuant outputs are available in the study repository https://github.com/UCLouvain-CBIO/2022-RSK-Nups-VIRO

Codes: Processed data and reproducible proDA analyses scripts are available in the study repository at https://github.com/UCLouvain-CBIO/2022-RSK-Nups-VIRO

# References


1 Sorgeloos, F. *et al.* A case of convergent evolution: Several viral and bacterial pathogens hijack RSK kinases through a common linear motif. *Proc Natl Acad Sci U S A* **119** (2022). https://doi.org:10.1073/pnas.2114647119

2 Alexa, A. *et al.* A non-catalytic herpesviral protein reconfigures ERK-RSK signaling by targeting kinase docking systems in the host. *Nat Commun* **13**, 472 (2022). https://doi.org:10.1038/s41467-022-28109-x

3 Chung, L. K. *et al.* The Yersinia Virulence Factor YopM Hijacks Host Kinases to Inhibit Type III Effector-Triggered Activation of the Pyrin Inflammasome. *Cell Host Microbe* **20**, 296-306 (2016). https://doi.org:10.1016/j.chom.2016.07.018

4 Ratner, D. *et al.* The Yersinia pestis Effector YopM Inhibits Pyrin Inflammasome Activation. *PLoS Pathog* **12**, e1006035 (2016). https://doi.org:10.1371/journal.ppat.1006035

5 Kuang, E., Fu, B., Liang, Q., Myoung, J. & Zhu, F. Phosphorylation of eukaryotic translation initiation factor 4B (EIF4B) by open reading frame 45/p90 ribosomal S6 kinase (ORF45/RSK) signaling axis facilitates protein translation during Kaposi sarcoma-associated herpesvirus (KSHV) lytic replication. *J Biol Chem* **286**, 41171-41182 (2011). https://doi.org:10.1074/jbc.M111.280982

6 Li, X. *et al.* ORF45-Mediated Prolonged c-Fos Accumulation Accelerates Viral Transcription during the Late Stage of Lytic Replication of Kaposi's Sarcoma-Associated Herpesvirus. *J Virol* **89**, 6895-6906 (2015). https://doi.org:10.1128/jvi.00274-15

7 Freundt, E. C., Drappier, M. & Michiels, T. Innate Immune Detection of Cardioviruses and Viral Disruption of Interferon Signaling. *Front Microbiol* **9**, 2448 (2018). https://doi.org:10.3389/fmicb.2018.02448

8 Brahic, M., Bureau, J. F. & Michiels, T. The genetics of the persistent infection and demyelinating disease caused by Theiler's virus. *Annu Rev Microbiol* **59**, 279-298 (2005). https://doi.org:10.1146/annurev.micro.59.030804.121242

9 van Pesch, V., van Eyll, O. & Michiels, T. The leader protein of Theiler's virus inhibits immediate-early alpha/beta interferon production. *J Virol* **75**, 7811-7817 (2001). https://doi.org:10.1128/jvi.75.17.7811-7817.2001

10 Zoll, J., Melchers, W. J., Galama, J. M. & van Kuppeveld, F. J. The mengovirus leader protein suppresses alpha/beta interferon production by inhibition of the iron/ferritin-mediated activation of NF-kappa B. *J Virol* **76**, 9664-9672 (2002). https://doi.org:10.1128/jvi.76.19.9664-9672.2002

11 Hato, S. V. *et al.* The mengovirus leader protein blocks interferon-alpha/beta gene transcription and inhibits activation of interferon regulatory factor 3. *Cell Microbiol* **9**, 2921-2930 (2007). https://doi.org:10.1111/j.1462-5822.2007.01006.x

12 Borghese, F. & Michiels, T. The leader protein of cardioviruses inhibits stress granule assembly. *J Virol* **85**, 9614-9622 (2011). https://doi.org:10.1128/jvi.00480-11

13 Borghese, F., Sorgeloos, F., Cesaro, T. & Michiels, T. The Leader Protein of Theiler's Virus Prevents the Activation of PKR. *J Virol* **93** (2019). https://doi.org:10.1128/jvi.01010-19

14 Delhaye, S., van Pesch, V. & Michiels, T. The leader protein of Theiler's virus interferes with nucleocytoplasmic trafficking of cellular proteins. *J Virol* **78**, 4357-4362 (2004). https://doi.org:10.1128/jvi.78.8.4357-4362.2004

15 Lidsky, P. V. *et al.* Nucleocytoplasmic traffic disorder induced by cardioviruses. *J Virol* **80**, 2705-2717 (2006). https://doi.org:10.1128/jvi.80.6.2705-2717.2006

16 Lizcano-Perret, B. & Michiels, T. Nucleocytoplasmic Trafficking Perturbation Induced by Picornaviruses. *Viruses* **13**, 1210 (2021).

17 Porter, F. W. & Palmenberg, A. C. Leader-induced phosphorylation of nucleoporins correlates with nuclear trafficking inhibition by cardioviruses. *J Virol* **83**, 1941-1951 (2009). https://doi.org:10.1128/jvi.01752-08

18 Porter, F. W., Brown, B. & Palmenberg, A. C. Nucleoporin phosphorylation triggered by the encephalomyocarditis virus leader protein is mediated by mitogen-activated protein kinases. *J Virol* **84**, 12538-12548 (2010). https://doi.org:10.1128/jvi.01484-09

19 Ricour, C. *et al.* Inhibition of mRNA export and dimerization of interferon regulatory factor 3 by Theiler's virus leader protein. *J Gen Virol* **90**, 177-186 (2009). https://doi.org:10.1099/vir.0.005678-0

20 Bardina, M. V. *et al.* Mengovirus-induced rearrangement of the nuclear pore complex: hijacking cellular phosphorylation machinery. *J Virol* **83**, 3150-3161 (2009). https://doi.org:10.1128/jvi.01456-08

21 Aramburu, I. V. & Lemke, E. A. Floppy but not sloppy: Interaction mechanism of FG-nucleoporins and nuclear transport receptors. *Semin Cell Dev Biol* **68**, 34-41 (2017). https://doi.org:10.1016/j.semcdb.2017.06.026

22 Beck, M. & Hurt, E. The nuclear pore complex: understanding its function through structural insight. *Nat Rev Mol Cell Biol* **18**, 73-89 (2017). https://doi.org:10.1038/nrm.2016.147

23 Hampoelz, B., Andres-Pons, A., Kastritis, P. & Beck, M. Structure and Assembly of the Nuclear Pore Complex. *Annu Rev Biophys* **48**, 515-536 (2019). https://doi.org:10.1146/annurev-biophys-052118-115308

24 Hülsmann, B. B., Labokha, A. A. & Görlich, D. The permeability of reconstituted nuclear pores provides direct evidence for the selective phase model. *Cell* **150**, 738-751 (2012). https://doi.org:10.1016/j.cell.2012.07.019

25 Mishra, A., Sipma, W., Veenhoff, L. M., Van der Giessen, E. & Onck, P. R. The Effect of FG-Nup Phosphorylation on NPC Selectivity: A One-Bead-Per-Amino-Acid Molecular Dynamics Study. *Int J Mol Sci* **20** (2019). https://doi.org:10.3390/ijms20030596

26 Kim, D. I. *et al.* An improved smaller biotin ligase for BioID proximity labeling. *Mol Biol Cell* **27**, 1188-1196 (2016). https://doi.org:10.1091/mbc.E15-12-0844

27 Lobert, P. E., Escriou, N., Ruelle, J. & Michiels, T. A coding RNA sequence acts as a replication signal in cardioviruses. *Proc Natl Acad Sci U S A* **96**, 11560-11565 (1999). https://doi.org:10.1073/pnas.96.20.11560

28 Ahlmann-Eltze, C. & Anders, S. proDA: Probabilistic Dropout Analysis for Identifying Differentially Abundant Proteins in Label-Free Mass Spectrometry. *bioRxiv*, 661496 (2020). https://doi.org:10.1101/661496

29 Chen, R. H., Sarnecki, C. & Blenis, J. Nuclear localization and regulation of erk- and rsk-encoded protein kinases. *Mol Cell Biol* **12**, 915-927 (1992). https://doi.org:10.1128/mcb.12.3.915-927.1992

30 Allen, J. J. *et al.* A semisynthetic epitope for kinase substrates. *Nat Methods* **4**, 511-516 (2007). https://doi.org:10.1038/nmeth1048

31 Lopez, M. S., Kliegman, J. I. & Shokat, K. M. The logic and design of analog-sensitive kinases and their small molecule inhibitors. *Methods Enzymol* **548**, 189-213 (2014). https://doi.org:10.1016/b978-0-12-397918-6.00008-2

32 Ricour, C. *et al.* Random mutagenesis defines a domain of Theiler's virus leader protein that is essential for antagonism of nucleocytoplasmic trafficking and cytokine gene expression. *J Virol* **83**, 11223-11232 (2009). https://doi.org:10.1128/jvi.00829-09

33 Cornelis, G. R. & Wolf-Watz, H. The Yersinia Yop virulon: a bacterial system for subverting eukaryotic cells. *Mol Microbiol* **23**, 861-867 (1997). https://doi.org:10.1046/j.1365-2958.1997.2731623.x

34 McDonald, C., Vacratsis, P. O., Bliska, J. B. & Dixon, J. E. The yersinia virulence factor YopM forms a novel protein complex with two cellular kinases. *J Biol Chem* **278**, 18514-18523 (2003). https://doi.org:10.1074/jbc.M301226200

35 Hentschke, M. *et al.* Yersinia virulence factor YopM induces sustained RSK activation by interfering with dephosphorylation. *PLoS One* **5** (2010). https://doi.org:10.1371/journal.pone.0013165

36 De Jesús-González, L. A. *et al.* The Nuclear Pore Complex Is a Key Target of Viral Proteases to Promote Viral Replication. *Viruses* **13**, 706 (2021). https://doi.org:10.3390/v13040706

37 Saeed, M. *et al.* Defining the proteolytic landscape during enterovirus infection. *PLoS Pathog* **16**, e1008927 (2020). https://doi.org:10.1371/journal.ppat.1008927

38 Belov, G. A. *et al.* Bidirectional increase in permeability of nuclear envelope upon poliovirus infection and accompanying alterations of nuclear pores. *J Virol* **78**, 10166-10177 (2004). https://doi.org:10.1128/jvi.78.18.10166-10177.2004

39 Linder, M. I. *et al.* Mitotic Disassembly of Nuclear Pore Complexes Involves CDK1- and PLK1-Mediated Phosphorylation of Key Interconnecting Nucleoporins. *Dev Cell* **43**, 141-156.e147 (2017). https://doi.org:10.1016/j.devcel.2017.08.020

40 Kosako, H. *et al.* Phosphoproteomics reveals new ERK MAP kinase targets and links ERK to nucleoporin-mediated nuclear transport. *Nat Struct Mol Biol* **16**, 1026-1035 (2009). https://doi.org:10.1038/nsmb.1656

41 Dong, B., Niwa, M., Walter, P. & Silverman, R. H. Basis for regulated RNA cleavage by functional analysis of RNase L and Ire1p. *Rna* **7**, 361-373 (2001). https://doi.org:10.1017/s1355838201002230

42 Jnaoui, K. & Michiels, T. Adaptation of Theiler's virus to L929 cells: mutations in the putative receptor binding site on the capsid map to neutralization sites and modulate viral persistence. *Virology* **244**, 397-404 (1998). https://doi.org:10.1006/viro.1998.9134

43 Duke, G. M. & Palmenberg, A. C. Cloning and synthesis of infectious cardiovirus RNAs containing short, discrete poly(C) tracts. *J Virol* **63**, 1822-1826 (1989). https://doi.org:10.1128/jvi.63.4.1822-1826.1989

44 Cornilescu, C. C., Porter, F. W., Zhao, K. Q., Palmenberg, A. C. & Markley, J. L. NMR structure of the mengovirus Leader protein zinc-finger domain. *FEBS Lett* **582**, 896-900 (2008). https://doi.org:10.1016/j.febslet.2008.02.023

45 Chow, M. *et al.* Myristylation of picornavirus capsid protein VP4 and its structural significance. *Nature* **327**, 482-486 (1987). https://doi.org:10.1038/327482a0

46 Mertens, J. *et al.* Directly Reprogrammed Human Neurons Retain Aging-Associated Transcriptomic Signatures and Reveal Age-Related Nucleocytoplasmic Defects. *Cell Stem Cell* **17**, 705-718 (2015). https://doi.org:10.1016/j.stem.2015.09.001

47 Follenzi, A., Ailles, L. E., Bakovic, S., Geuna, M. & Naldini, L. Gene transfer by lentiviral vectors is limited by nuclear translocation and rescued by HIV-1 pol sequences. *Nat Genet* **25**, 217-222 (2000). https://doi.org:10.1038/76095

48 Hermant, P., Francius, C., Clotman, F. & Michiels, T. IFN-ε is constitutively expressed by cells of the reproductive tract and is inefficiently secreted by fibroblasts and cell lines. *PLoS One* **8**, e71320 (2013). https://doi.org:10.1371/journal.pone.0071320

49 Cesaro, T. *et al.* PKR activity modulation by phosphomimetic mutations of serine residues located three aminoacids upstream of double-stranded RNA binding motifs. *Sci Rep* **11**, 9188 (2021). https://doi.org:10.1038/s41598-021-88610-z

50 Bollaert, E. *et al.* HBP1 phosphorylation by AKT regulates its transcriptional activity and glioblastoma cell proliferation. *Cell Signal* **44**, 158-170 (2018). https://doi.org:10.1016/j.cellsig.2018.01.014

51 Tossounian, M. A. *et al.* Methionine sulfoxide reductase B from Corynebacterium diphtheriae catalyzes sulfoxide reduction via an intramolecular disulfide cascade. *J Biol Chem* **295**, 3664-3677 (2020). https://doi.org:10.1074/jbc.RA119.012438

52 Cox, J. & Mann, M. MaxQuant enables high peptide identification rates, individualized p.p.b.-range mass accuracies and proteome-wide protein quantification. *Nat Biotechnol* **26**, 1367-1372 (2008). https://doi.org:10.1038/nbt.1511

53 Benjamini, Y. & Hochberg, Y. Controlling the False Discovery Rate: A Practical and Powerful Approach to Multiple Testing. *Journal of the Royal Statistical Society. Series B (Methodological)* **57**, 289-300 (1995).

## Acknowledgments

We are grateful to Melissa Drappier for suggesting the analog-sensitive kinase experiments. We are much indebted to Kevan Shokat for quick support and detailed protocols concerning this great technique. We thank Frank J.M. van Kuppeveld for the gift of anti-EMCV capsid antibodies. We thank Stéphane Messe for excellent technical assistance, Nicolas Dauguet for expert help in cell sorting, and Eric Freundt and Frank J.M. van Kuppeveld for critical reading of this manuscript.

## Author Contributions

Conceptualization: B.L.P. and T.M.

Methodology: B.L.P, C.L., D.V., F.S. and T.M.

Formal analysis: P.H., F.S., L.G.

Investigation: B.L.P, F.W., G.H., D.V. and T.M.

Writing – original draft: B.L.P.

Writing – review & editing: B.L.P., D.V., F.S. and T.M.

Supervision: T.M.

Project administration: T.M.

Funding acquisition: T.M.

**Competing interests**

The authors declare no conflicts of interests

**Funding**

BLP and CL were the recipients of FRIA fellowship from the belgian FNRS. Work was supported by the EOS joint programme of Fonds de la recherche scientifique-FNRS and Fonds wetenschappelijk onderzoek-Vlaanderen-FWO (EOS ID: 30981113 and 40007527), Belgian fund for Scientific Research (PDR T.0185.14), Loterie Nationale through support to the de Duve Institute and Actions de Recherches Concertées (ARC).

# Figure legends

**Fig 1. Pathogen's proteins hijack RSK kinases.**

(A) Indirect substrate recruitment - model of the clamp: a pathogen's protein acts as an adaptor protein, which binds and activates RSK through its DDVF motif and recruits a target

protein to be phosphorylated by RSK through another domain. (B) Direct substrate recruitment. A pathogen's protein interacts with RSK through its DDVF motif and is directly phosphorylated by RSK.

**Fig 2. PTB diffusion and NUP98 hyperphosphorylation induced by cardioviruses depends on both the L protein and RSK kinases.**

(A-C and E-G) PTB diffusion out of the nucleus depends on both L and RSK. (A and E) Confocal microscopy images of HeLa WT cells infected with TMEV for 10h (A) or with EMCV for 4h (E). (B and F) Graphs showing the percentage of cells with PTB diffusion (mean ± SD), among cells infected by TMEV (3D-positive) for 10h (B) or by EMCV (capsid-positive) for 5h (F). Counts: 25-50 infected cells per experiment (n=4). **** denotes significant differences (One-way ANOVA, $p < 0.0001$) between HeLa-RSK-TKO cells transduced with an empty vector (HeLa TKO) and cells re-expressing indicated RSK isoforms, for $L^{WT}$-infected samples. (C and G) Confocal microscopy images of HeLa-WT or HeLa RSK-TKO cells transduced with an empty vector (HeLa TKO) or re-expressing the indicated RSK isoforms. Cells were infected with TMEV for 10h (C) or EMCV for 4h (G). 3D and 2A were stained as controls of TMEV and EMCV infection respectively. (D and H) Western blots showing the RSK-dependent hyperphosphorylation of NUP98 (shift upwards) or the inhibition of PKR activation induced by TMEV (D) or EMCV (H). 3D or 2A were detected as control of infection, and ß-actin as loading control. Dashed lines between lanes indicate deletion of irrelevant sections from the same membrane.

**Fig 3. Nucleocytoplasmic traffic perturbation in live cells depends on both the L protein and RSK kinases.**

(A-D) Graphs and confocal microscopy pictures showing the quantification of RFP-NLS and GFP-NES diffusion (mean ± SD) in live HeLa-LVX cells infected with TMEV for 10h (A-B) or EMCV for 4h30 (C-D). HeLa-LVX cells were either WT, or RSK-TKO cells transduced with an empty vector (HeLa-TKO) or re-expressing RSK1. Counts: 50 cells per experiment (n=4). (E-G) Impact of L on nucleocytoplasmic traffic. HeLa-LVX cells transfected with an empty plasmid or with plasmids expressing $L^{WT}$, L mutants or YopM. (E) Confocal microscopy of HeLa-LVX cells 24hours post-transfection. (F) Western blot of HeLa-LVX cells 24h post-transfection. FLAG staining shows the expression of L proteins and YopM. (G) Graph showing the percentage of cells with GFP-NES and RFP-NLS diffusion (mean ± SD). Counts: 70±5 cells per experiment (n=6). One-way ANOVA test was used to compare all samples to $L^{WT}$. **** denotes significant differences (One-way ANOVA, $p < 0.0001$). Scale bar: 20µm

**Fig 4. BioID-RSK and BioID-L fusion proteins biotinylate specific proteins during cardiovirus infection.**

(A) Cartoon showing the expected biotinylation by BioID-RSK or BioID-L fusion proteins of a target recruited by the C-terminal domain of L. (B) Western blot of proteins biotinylated by BioID-RSK in lysates and pulled down samples of TMEV infected cells. HeLa BioID-RSK cells were incubated for 2 days without biotin. Cells were then infected for 16h (MOI 2.5) with $L^{WT}$ or $L^{M60V}$ viruses in medium containing 5µM biotin. Biotinylated proteins were pulled-down using streptavidin-magnetic beads. (C) Schematic representation of BioID-L TMEV replicon constructs. Capsid protein sequences were replaced by BioID-L and GFP sequences. The beginning of the VP4 sequence was kept in order to allow BioID-L protein processing by viral protease 3C, and the CRE sequence (localized in VP2) was added to allow replication. (D) Western blot of proteins biotinylated by BioID-L in lysates and pulled

down samples of TMEV infected cells. HeLa cells were infected for 14h (MOI 2.5) with BioID-$L^{WT}$, BioID-$L^{M60V}$ or BioID-$L^{F48A}$ replicons in medium containing 5µM biotin. Biotinylated proteins were then pulled-down using streptavidin-magnetic beads.

**Fig 5. BioID-RSK and BioID-L proxeomes identify FG-NUPs as targets recruited by the L-RSK complex.**

(A) Proteins identified in the proximity of BioID-RSK (y axis) and BioID-L (x axis). Y-axis shows proteins detected after infection with $L^{WT}$ but not $L^{M60V}$ viruses (=PSMs in $L^{WT}$/($L^{M60V}$+NI+1)). X-axis shows proteins detected after infection with BioID-$L^{WT}$ or BioID-$L^{F48A}$ but not BioID-$L^{M60V}$ replicons (= PSMs in ($L^{WT}$+ $L^{F48A}$)/( $L^{M60V}$+NI+1)). FG-NUPs are identified by green dots. (B) Table showing the adjusted P-values for the 20 best ranked proteins. Ranking was attributed by multiplying the BioID-RSK ratio by the BioID-L ratio. Statistical analysis of pairwise comparisons made between $L^{WT}$ and $L^{M60V}$ for BioID-RSK and between $L^{WT}$ and $L^{M60V}$ or $L^{F48A}$ and $L^{M60V}$ for BioID-L. Adjusted P-values < 0.05 are colored in red, FG-NUPs are colored in green. (C) Volcano plots showing the same pairwise comparisons as in B. Proteins having an adjusted P-value < 0.05 and a $Log_2$ fold change (LFC) > 1 are colored in red (= proteins in Q2). FG-NUPs are colored in green.

**Fig 6. Subcellular localization of proteins biotinylated by BioID-RSK.**

(A) Confocal microscopy images of biotinylated proteins (green) and 3D viral polymerase (red) detected in BioID-RSK expressing HeLa cells infected with $L^{WT}$ or $L^{M60V}$ viruses for 10h (MOI 5). (B) Quantification of cells showing a visible nuclear rim of biotinylated proteins in HeLa BioID-RSK cells infected with $L^{WT}$ or $L^{M60V}$ viruses (mean ± SD). Counts: 42 ± 10 infected cells per experiment (n=4). One-way ANOVA tests were used to compare all samples with each other, **** denotes significant differences (p < 0.0001). (C) BioID-

RSK biotinylates proteins that colocalize with the FG-NUP NUP98. Confocal microscopy images of biotinylated proteins (green), 3D viral polymerase (red), and NUP98 (orange) in HeLa BioID-RSK cells infected with $L^{WT}$ or $L^{M60V}$ viruses for 10h (MOI 5). 3D viral polymerase was stained as a control of infection. White arrows point to examples of cells exhibiting a nuclear rim staining. Scale bar: 10µm.

**Fig 7. Subcellular localization of proteins biotinylated by BioID-L.**

(A) Confocal microscopy images of biotinylated proteins stained with streptavidin-Alexa Fluor 594 (orange) and 3D viral polymerase (green) in HeLa cells infected for 10h with BioID-$L^{WT}$, BioID-$L^{M60V}$ or BioID-$L^{F48A}$ replicons (MOI 5). (B) Quantification of nuclear rim staining in HeLa cells infected with BioID-$L^{WT}$, BioID-$L^{M60V}$ or BioID- $L^{F48A}$ viruses (mean ± SD). Counts: 31 ± 11 infected cells per experiment (n=4). One-way ANOVA tests were used to compare all samples with each other, **** denotes significant differences ($p < 0.0001$). 3D viral polymerase was stained as a control of infection. (C) BioID-L biotinylates proteins that colocalize with the FG-NUP POM121. Confocal microscopy images of biotinylated proteins (orange) and POM121 (green) in HeLa cells infected with BioID-$L^{WT}$, BioID-$L^{M60V}$ or BioID-$L^{F48A}$ viruses for 10h (MOI 5). White arrows point to examples of cells exhibiting a nuclear rim staining. Scale bar: 10µm.

**Fig 8. RSK directly phosphorylates NUP98 in TMEV and EMCV infected cells.**

(A) Cartoon showing the principle of the analog-sensitive kinase system. The kinase mutated in the ATP binding pocket (As-RSK) can use regular ATP as well as a bulkier ATP analog (A*TP-S). Use of the ATP analog induces the thiophosphorylation of the substrate. After an alkylation reaction with paranitrobenzylmesylate (PNBM), thiophosphates are converted to thiophosphate esters, which are specifically recognized by an anti-thiophosphate ester

antibody. All other wild-type kinases in the cell, have normal ATP binding pockets that cannot accommodate the ATP analog. (B) Identification of the gatekeeper residue in RSK2. The gatekeeper residue of RSK2 was identified by aligning the sequences of c-SRC (P00523) with those of the N-terminal kinase domain of RSKs (RSK1: Q15418, RSK2: P51812, RSK3: Q15349, RSK4: Q9UK32). Typically, the gatekeeper residue aligns with T338 of c-SRC, and is preceded by two hydrophobic amino acids and followed by an acidic and another hydrophobic amino acid. RSK2 gatekeeper residue was thereby identified as L147. (C-E) HeLa cells expressing As2-RSK or WT-RSK were infected with TMEV for 8h (MOI 5) (C and E) or with EMCV for 3h30min (MOI 5) (D). Cells were then permeabilized with digitonin, and N6-Bn-ATP-γ-S was added for 1 hour. Cells were then lysed and either NUP98 (C and D) or thio-phosphate-ester containing proteins were immunoprecipitated (E). (C and D) Immunoblots showing a concentrated amount of NUP98 in the immunoprecipitation samples and thiophosphate-ester proteins. (E) Immunoblots showing NUP98 in the thiophosphate ester IP fraction when $L^{WT}$ is present. Detection of viral capsid in the lysates was made as control for infection.

Fig. 1

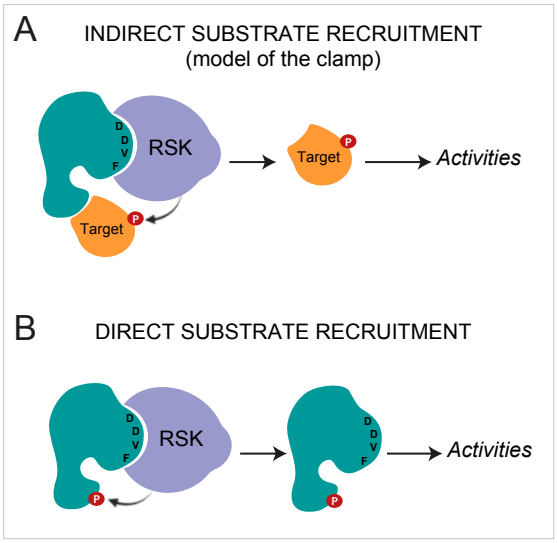

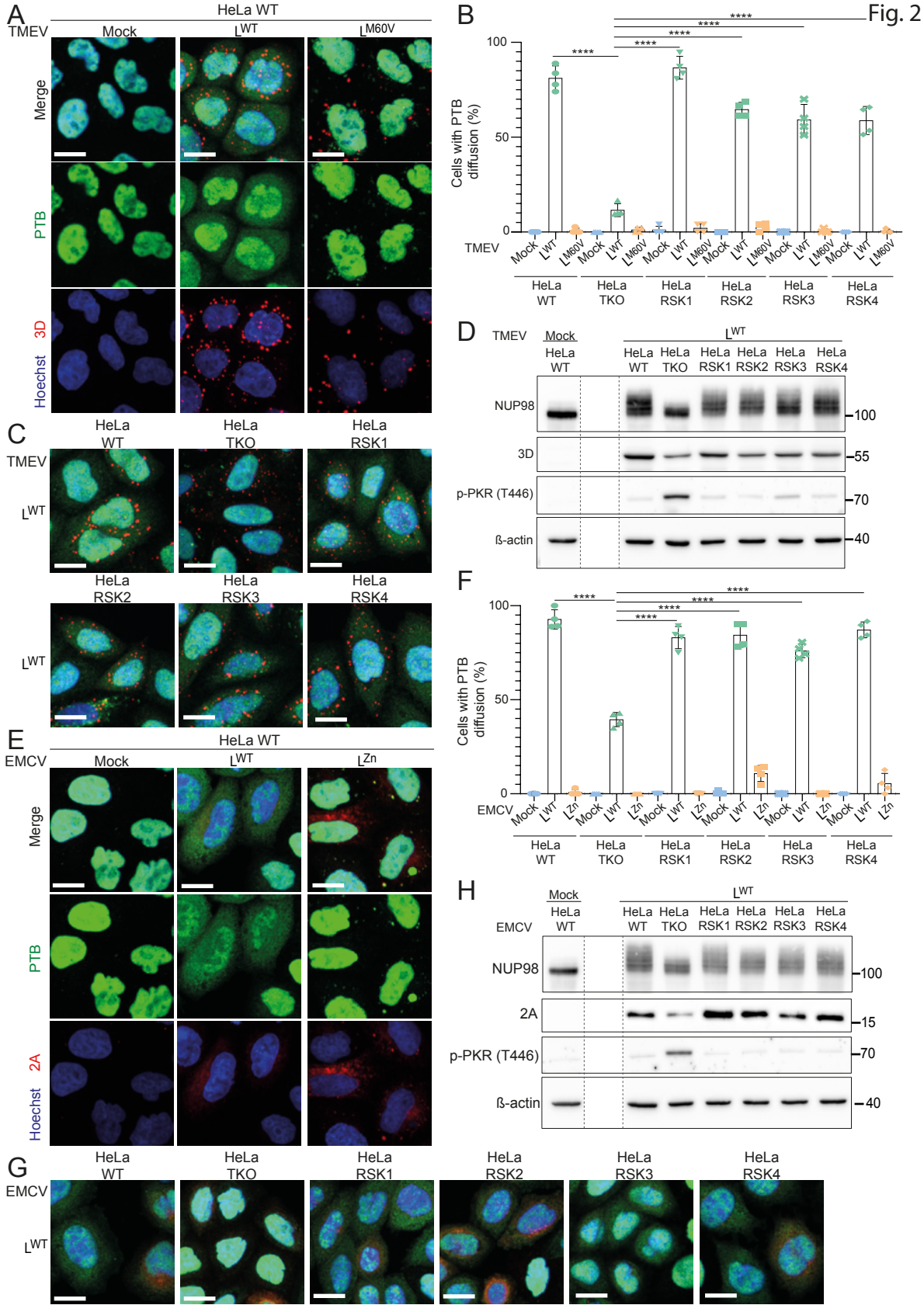

Fig. 3

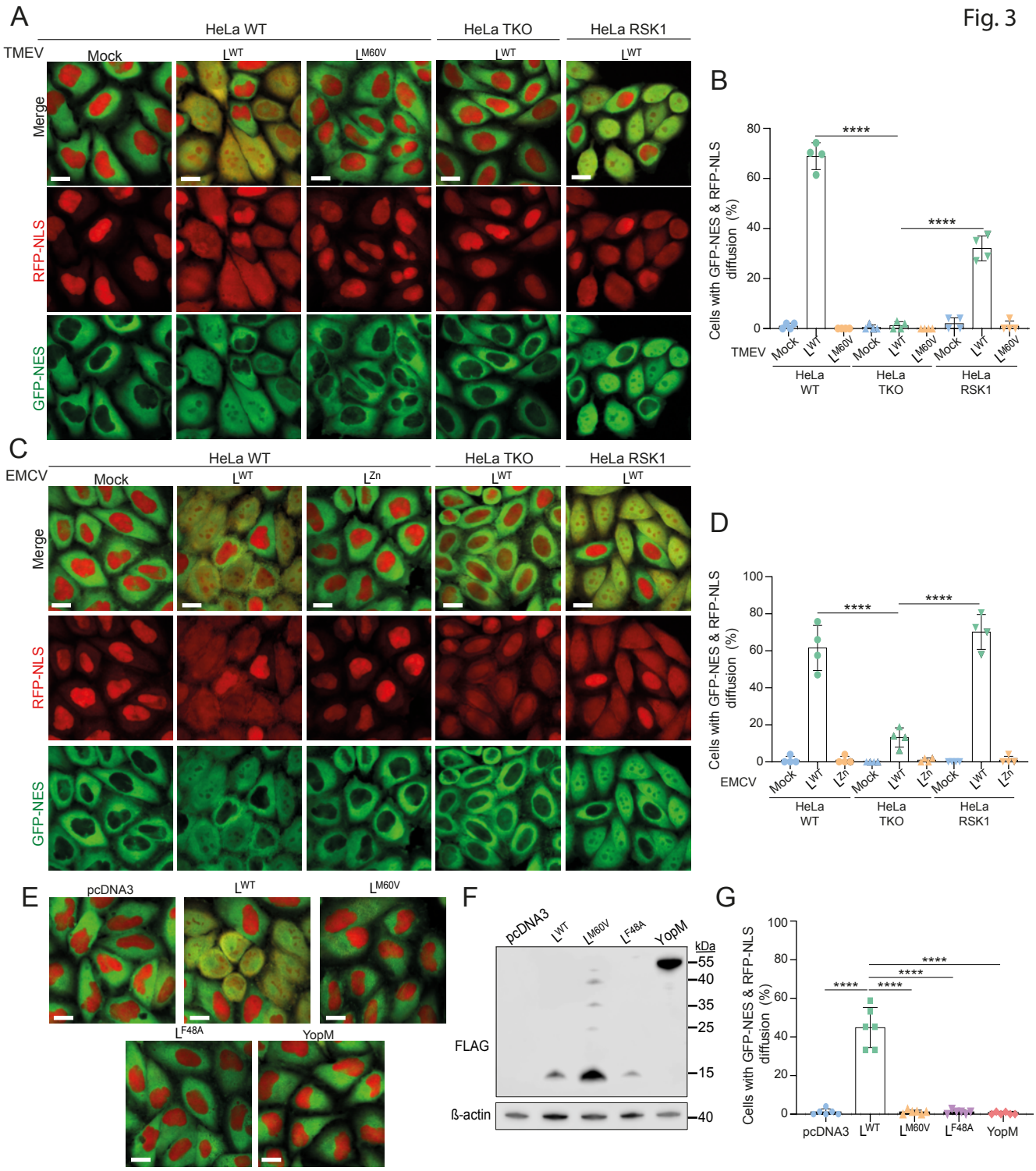

Fig. 4

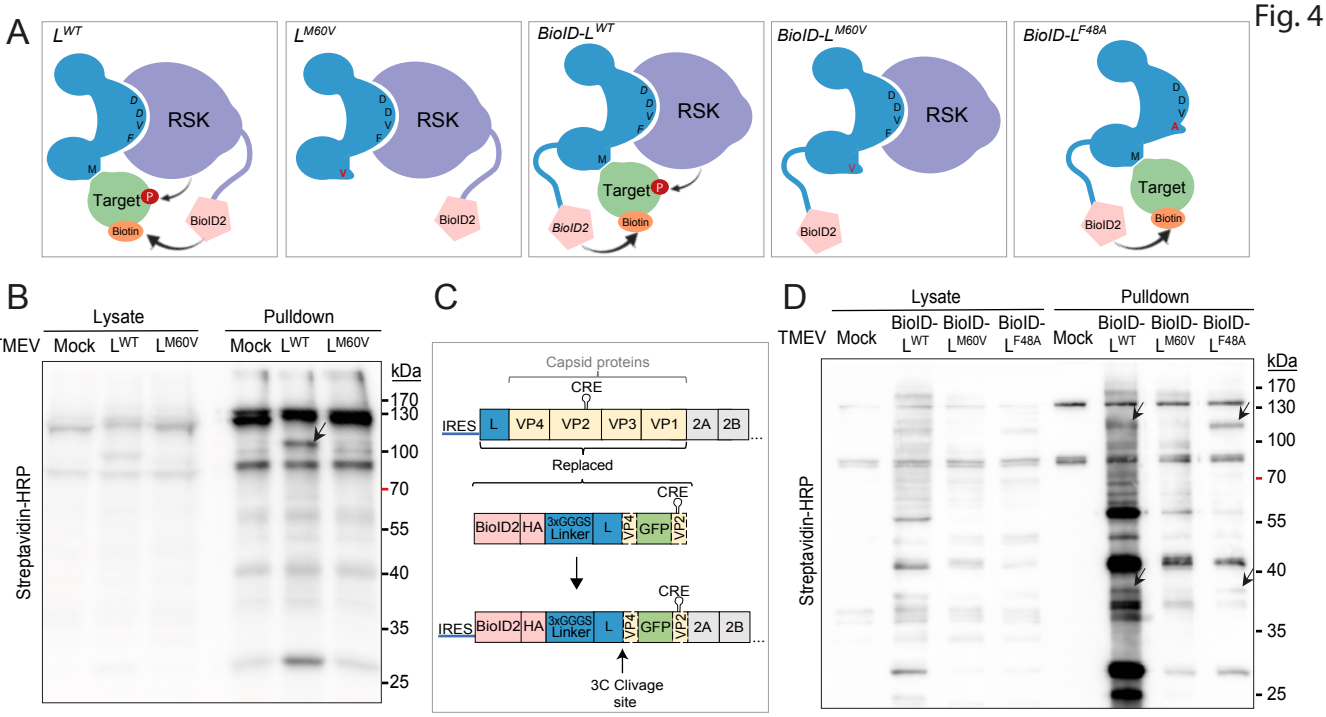

A

Fig. 5

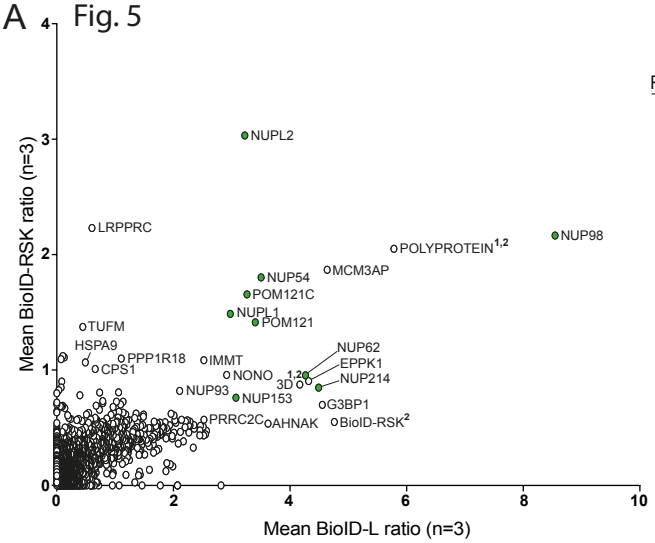


B

| Ranking | BioID-RSK ratio x BioID-L ratio | Gene name | BioID-RSK ratio (mean) | BioID-L ratio (mean) | Adj. P-value BioID-RSK $L^{WT}$ vs $L^{M60V}$ | Adj. P-value BioID-L $L^{WT}$ vs $L^{M60V}$ | Adj. P-value BioID-L $L^{F48A}$ vs $L^{M60V}$ |
|---|---|---|---|---|---|---|---|
| 1 | 18.51 | NUP98 | 2.17 | 8.55 | 0.558 | 0.003 | 0.001 |
| 2 | 11.85 | POLYPROTEIN[1,2] | 2.05 | 5.78 | NA | NA | NA |
| 3 | 9.78 | NUPL2 | 3.03 | 3.22 | 0.429 | 0.081 | 0.740 |
| 4 | 8.67 | MCM3AP | 1.87 | 4.64 | 0.614 | 0.003 | 0.001 |
| 5 | 6.32 | NUP54 | 1.80 | 3.51 | 0.827 | 0.039 | 0.112 |
| 6 | 5.40 | POM121C | 1.66 | 3.26 | 0.429 | 0.057 | 0.192 |
| 7 | 4.81 | POM121 | 1.41 | 3.40 | 0.827 | 0.032 | 0.085 |
| 8 | 4.43 | NUPL1 | 1.49 | 2.98 | 0.614 | 0.015 | 0.007 |
| 9 | 4.07 | NUP62 | 0.95 | 4.26 | 0.558 | 0.015 | 0.007 |
| 10 | 3.91 | EPPK1 | 0.90 | 4.32 | 0.827 | 0.033 | 0.975 |
| 11 | 3.81 | NUP214 | 0.85 | 4.49 | 0.827 | 0.015 | 0.002 |
| 12 | 3.64 | 3D[1,2] | 0.87 | 4.17 | NA | NA | NA |
| 13 | 3.18 | G3BP1 | 0.70 | 4.55 | 0.827 | 0.015 | 0.493 |
| 14 | 2.79 | NONO | 0.96 | 2.91 | 0.827 | 0.062 | 0.839 |
| 15 | 2.74 | IMMT | 1.09 | 2.52 | 0.827 | 0.028 | 0.740 |
| 16 | 2.62 | BIOID-RSK2[2] | 0.55 | 4.76 | NA | NA | NA |
| 17 | 2.34 | NUP153 | 0.76 | 3.07 | 0.827 | 0.024 | 0.024 |
| 18 | 1.94 | AHNAK | 0.54 | 3.62 | 0.903 | 0.237 | 0.813 |
| 19 | 1.73 | NUP93 | 0.82 | 2.11 | 0.827 | 0.081 | 0.493 |
| 20 | 1.44 | PRRC2C | 0.57 | 2.52 | 0.827 | 0.045 | 0.916 |

[1] Viral proteins
[2] Data of identified peptides belonging to shared protein groups.

C

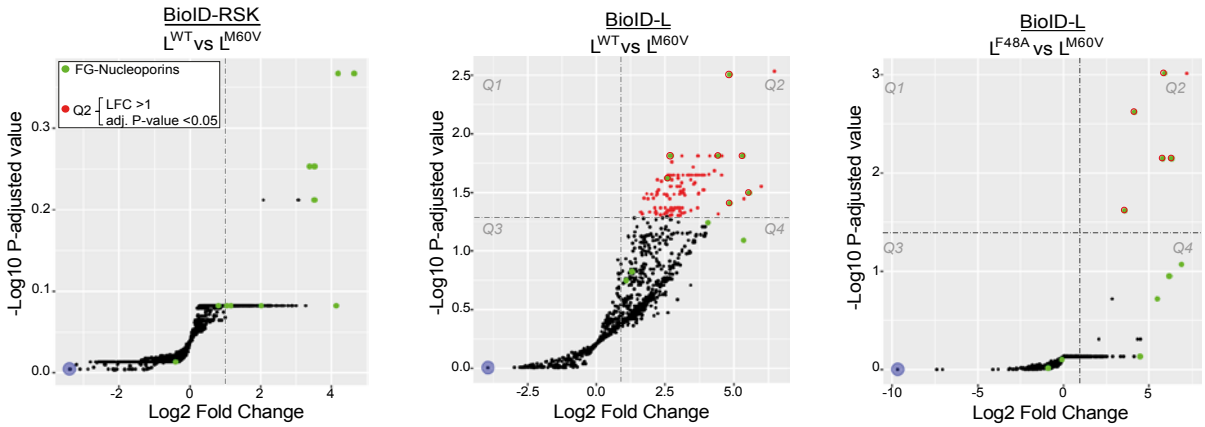

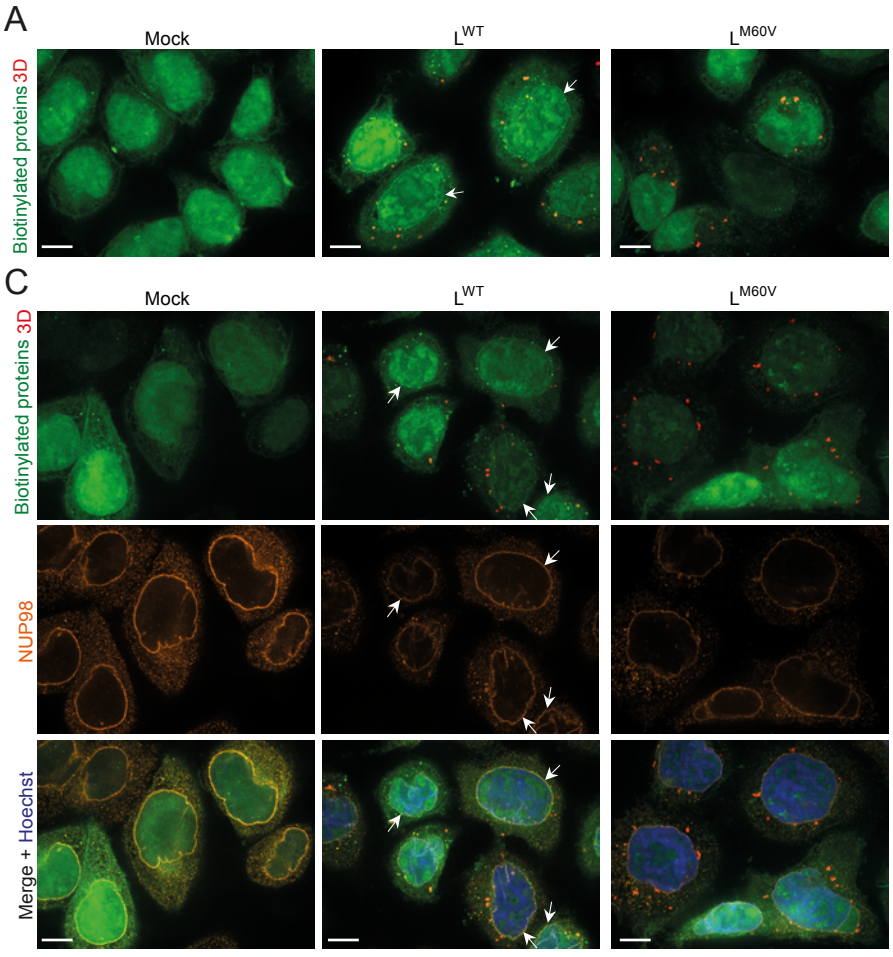


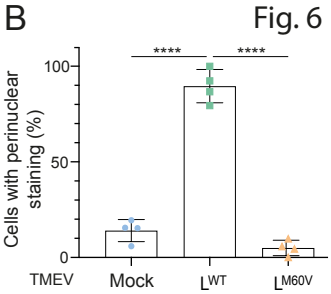

Fig. 7

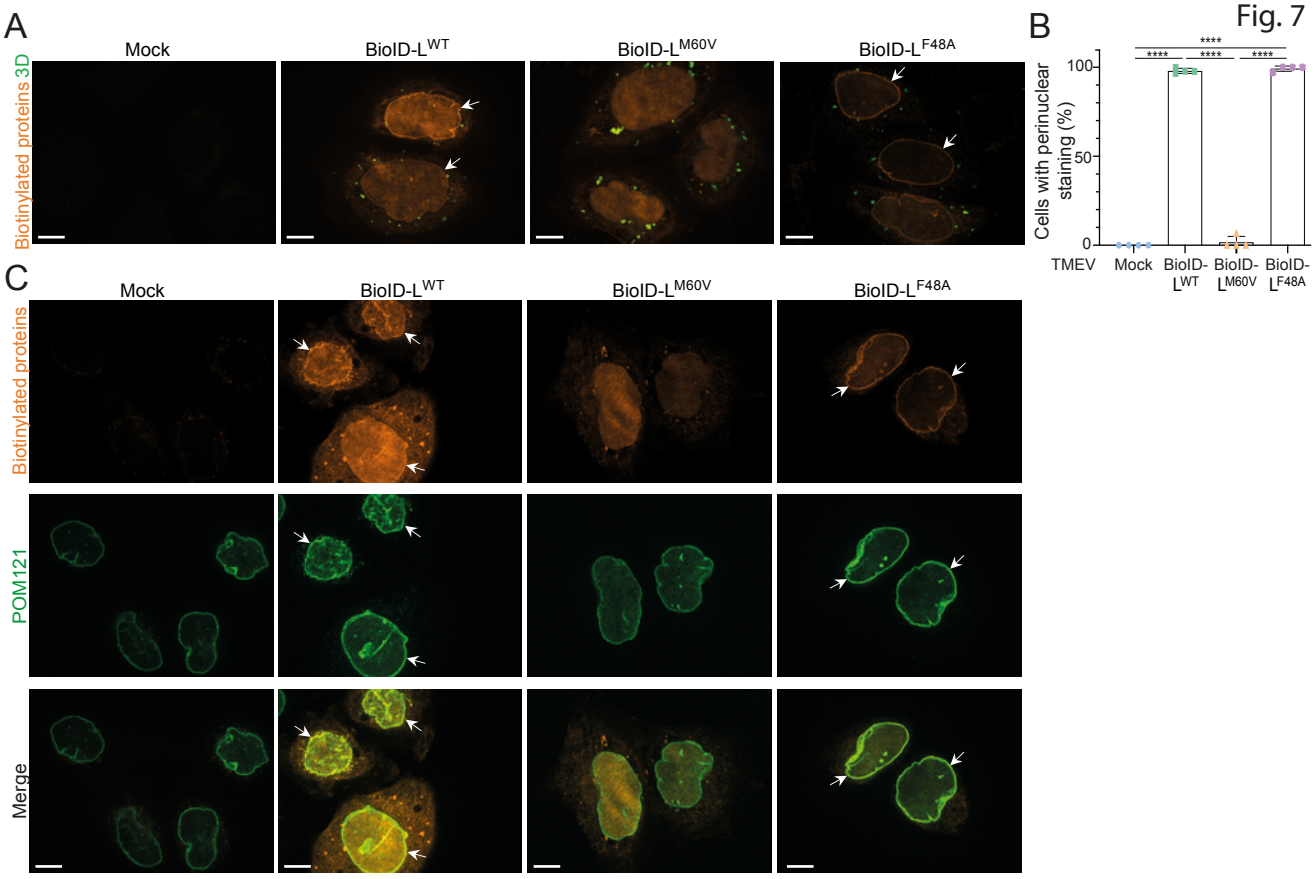

Fig. 8